SSRG International Journal of Mechanical Engineering
ISSN: 2348-8360/ https://doi.org/10.14445/23488360/IJME-V13I10P110

Volume 13 Issue 10, 139-157, October 2026
© 2026 Seventh Sense Research Group®

Original Article

Thermo-Physical and Mechanical Characterisation of Pumice-Kaolin Composite Refractories with Multi-Objective Optimisation for Thermal Insulation Applications

James Audu[1*], Abdulrahman Asipita Salawu[2], Muriana Rasheed Aremu[3], Abdullahi Aliyu Alhaji[4], Lawal Sadiq Sius[5]

[1,4,5]*Department of Mechanical Engineering, School of Infrastructure, Process Engineering and Technology, Federal University of Technology Minna, Niger State, Nigeria.*

[2,3]*Department of Materials and Metallurgical Engineering, School of Infrastructure, Process Engineering and Technology, Federal University of Technology Minna, Niger State, Nigeria.*

[1]*Corresponding Author: james.audu@st.futminna.edu.ng*

Received: 21 August 2026 Revised: 14 October 2026 Accepted: 20 October 2026 Published: 26 October 2026

Abstract *- Pumice-kaolin composites were produced from Nigerian raw materials to examine how pumice content (25, 50 and 75 wt%) and pumice particle size (75, 150 and 300 µm) affect the balance between thermal insulation and strength in fired refractories. A two-factor Taguchi L9 design was used, and all specimens were fired at 1200 °C for 1 h. Bulk density ranged from 1.44 to 2.00 g/cm^3, as-fired flexural strength from 0.18 to 0.95 MPa and apparent thermal conductivity at a nominal 1000 °C from 1.33 to 1.68 W/m·K. Two formulations failed an apparent specific gravity check and were excluded from the analyses that use porosity or bulk density. No test cone deformed up to a kiln temperature of 1200 °C. Particle size governed thermal conductivity (85.8% contribution, p = 0.001). Grey relational analysis of the seven retained runs gave the highest grade to 25 wt% pumice with 75 µm particles (0.734; first in ten of thirteen sensitivity scenarios), and factor-level analysis placed the preferred region at 25 wt% pumice with 75 to 150 µm particles. The composites do not meet ASTM C155 limits for insulating firebrick, and their use as backup lining requires confirmation by replicated, load and service tests.*

Keywords *- Composite refractories, Grey Relational Analysis, Pumice-kaolin, Taguchi design, Thermal insulation.*

1. Introduction

Furnace and kiln linings largely decide how much fuel a thermal process consumes, how quickly it can be heated and cooled, and how long it runs before relining [1, 2]. In service, the lining is exposed to high temperature, chemical attack by slags and gases, and repeated mechanical and thermal loading [3-5]. Where a lining layer is intended to insulate, it is judged mainly on two losses: the heat that flows through the wall while the furnace operates, and the heat absorbed by the lining that is lost each time the furnace cools. Both losses are controlled by the density, pore structure and phase assemblage of the fired body [6, 7].

Most refractory shapes used by Nigerian foundries, heat-treatment workshops and ceramic kilns are imported, and their cost is a particular burden for small operators [8, 9]. Kaolin, by contrast, is abundant locally. Reserves at Ikere-Ekiti have been put at about 2.7 million tonnes, and published analyses of this kaolin give 32 to 36 wt% Al_2O_3 [10, 11]. Nigerian clays have been developed into aluminosilicate crucibles [9, 10] and additive-modified refractory bodies [12], and insulating bricks have been produced by burning out sawdust or melon seed husk to create pores [13, 14]. In the sawdust work, a kaolinite brick of 1.81 g/cm^3 conducted 1.65 W/m·K, and adding 40% sawdust reduced the density to 1.29 g/cm^3 and the conductivity to 1.48 W/m·K [14]. Organic pore formers are effective, yet they require a burn-out stage, release gases during firing and tie production to a second raw material whose supply may vary.

Natural pumice offers a mineral route to porosity. This vesicular volcanic glass usually contains 60 to 75 wt% SiO_2, 13 to 17 wt% Al_2O_3 and 7 to 8 wt% Na_2O plus K_2O [15, 16]. As an aggregate in concrete, geopolymers and floor fills it reduces density and conductivity, although strength falls as well [17-20], and its grain size alters packing and pozzolanic

This is an open access article under the CC BY-NC-ND license (http://creativecommons.org/licenses/by-nc-nd/4.0/)

reactivity [21]. Fired clay bricks behave in a similar way: 40 wt% pumice lowered conductivity from 0.96 to below 0.65 W/m·K [22], and a pumice-vermiculite addition reduced density from 1.93 to 1.31 g/cm^3 and conductivity from 1.041 to 0.439 W/m·K while compressive strength dropped by 24% [23].

Those were building bricks, fired at 900 to 1000 °C and measured at room temperature. When the firing temperature rises to 1200 °C, the alkalis in pumice behave as fluxes and can change the proportions of glass and mullite that develop in a kaolin matrix [24, 25].

In such bodies, kaolin provides plasticity and green strength and, on firing, an aluminosilicate bond containing mullite [25, 26]; for this reason, it is the base of many clay-bonded refractories and ceramic composites [27-29]. Designing an insulating refractory is therefore a matter of compromise. Pores lower the effective conductivity but remove the solid that carries load [5, 30, 31], and the outcome depends not only on pore volume but also on pore size, connectivity and the moisture retained in open pores [30, 32, 33].

Where several responses conflict, Taguchi orthogonal arrays, Analysis of Variance (ANOVA) and Grey Relational Analysis (GRA) are widely used [34-36], for example, to balance porosity and strength in metakaolin geopolymers [37] and to select blended mortar mixes [38]. Many such studies, however, report a single grey relational grade without examining factor-level effects, without making clear that a predicted optimum drawn from the same data set is only an internal fit check, and without showing whether the ranking survives changes in weights, normalisation or the distinguishing coefficient [38].

The studies closest to the present work are compared in Table 1, and four gaps emerge from them. The combined effect of pumice content and pumice particle size on a kaolin-bonded body fired at refractory temperature has not been examined systematically. Data on pumice-clay bodies are limited to the room-temperature conductivity of building bricks, whereas furnace linings operate at 800 to 1200 °C. Nigerian refractory products are seldom compared with ASTM C155 [39] or with commercial insulating firebrick. Finally, multi-response selections in this field are rarely tested for robustness or for the influence of doubtful measurements.

Table 1. Summary of closely related studies and the gap addressed in this work

Study	Material system and firing	Main reported findings	Analysis	Gap relative to the present aim
Gencel [22]	Brick clay with up to 40 wt% pumice; 900 and 1000 °C	k fell from 0.96 to below 0.65 W/m·K at 40 wt% pumice	One factor	Building brick; room-temperature k; no refractory tests
Koçyiğit [23]	Clay with 10 to 40 wt% pumice and 5% vermiculite; 950 °C	Density 1.93 to 1.31 g/cm^3; k 1.041 to 0.439 W/m·K; strength fell 24%	One factor	Low firing temperature; particle size not varied
Mgbemene et al. [14]	Nigerian kaolinite clay with sawdust or iron filings; 900 to 1200 °C	Density 1.81 to 1.29 g/cm^3; k 1.65 to 1.48 W/m·K (0 to 40% sawdust)	Data set	No strength, refractoriness or optimisation
Odewole et al. [10]	Ikere kaolin, ball clay, grog and Awo quartz crucibles; 1300 °C	Water absorption 0.36 to 0.72%; compressive strength 1.43 to 1.65 MPa	Mix comparison	Dense bodies; insulation not addressed
Al-Sultani et al. [37]	Metakaolin geopolymer foam; not fired	Taguchi-GRA balanced porosity and compressive strength	Taguchi-GRA	Not a refractory; no sensitivity check
Nam et al. [38]	Quaternary blended mortar	Multi-response mix selection by Taguchi-GRA	Taguchi-GRA	Cementitious system; ambient service
Present study	Ikere kaolin with Nigerian pumice, 25 to 75 wt% and 75 to 300 µm; 1200 °C	Physical, mechanical, thermal (800 to 1200 °C) and PCE responses	S/N, full ANOVA, GRA, factor-level analysis, sensitivity	Benchmarked against ASTM C155 and commercial firebrick

The present study addresses these gaps for pumice-kaolin composites made from Nigerian raw materials, with pumice content and particle size varied in a two-factor L9 design. The contribution does not lie in the statistical tools. It lies in a combined physical, mechanical, thermal and refractoriness data set for this material system; in a multi-response evaluation that reports every intermediate step, screens out measurements that fail a physical consistency check and tests the result in thirteen sensitivity scenarios; and in a benchmark against ASTM C155, commercial insulating firebrick and

published clay composites, accompanied by an indicative estimate of lining heat flux. The limitations of the data are stated alongside each result so that the conclusions can be read with the appropriate degree of confidence.

2. Materials and Methods

2.1. Raw Materials

The pumice was sourced in Niger State, and the kaolin at Ikere-Ekiti, Ekiti State, Nigeria. Pumice lumps were crushed, milled and sieved to give three fractions of 75, 150 and 300 µm. The kaolin was soaked in water, passed wet through a 150 µm sieve to separate sand and organic matter, and dried in air.

2.1.1. Chemical and Mineralogical Profile of the Raw Materials

X-ray Fluorescence (XRF) and X-ray Diffraction (XRD) were not carried out on the batches used in this programme. To give the reader a chemical basis for interpreting the results, Table 2 collects published oxide analyses of Ikere-Ekiti kaolin and the typical composition range of natural pumice.

These values describe the deposits and material class, not the exact batches tested here, and they are used only for the estimates in Table 3.

Table 2. Published oxide composition of the raw material sources

Oxide (wt%)	Ikere kaolin [10]	Ikere kaolin [11]	Pumice, typical [15]
SiO_2	58.60	46.38	60 to 75
Al_2O_3	32.30	36.10	13 to 17
Fe_2O_3	1.21	0.58	1 to 3
CaO	n.r.	0.05	1 to 2
MgO	n.r.	0.07	Low
Na_2O	0.86	0.86	7 to 8
K_2O	3.46	0.46	
TiO_2	0.11	0.72	Low
LOI	3.43	13.07	n.r.
Al_2O_3/SiO_2	0.55	0.78	0.17 to 0.28

n.r. = not reported; LOI = loss on ignition. For pumice, the 7 to 8 wt% range refers to $Na_2O + K_2O$ combined.

The two kaolin analyses differ mainly in loss on ignition and potassium. The sample with 13.07% LOI and 36.1% Al_2O_3 is close to ideal kaolinite, whereas the one with 3.43% LOI and 3.46% K_2O appears to contain mica or feldspar and some quartz. Both have low iron and titania, which is favourable for refractoriness.

The theoretical Al_2O_3/SiO_2 mass ratio of kaolinite is about 0.85; the reported ratios of 0.55 and 0.78 indicate free silica in addition to kaolinite. Pumice brings much more silica and several times more alkali than kaolin, so each increase in pumice content lowers the alumina available for mullite and raises the flux content of the body.

Using the mean of the two kaolin analyses and the mid-points of the pumice ranges, the approximate oxide chemistry of each blend was estimated by the lever rule. The upper limit of mullite ($3Al_2O_3{\cdot}2SiO_2$, 71.8 wt% Al_2O_3) that the kaolin fraction can form on a calcined basis was estimated with Equation (1), in which x_p is the pumice mass fraction, and LOI_k is the kaolin loss on ignition. Pumice alumina was excluded because it is tied up in an alkali-rich glass.

$$M_{\max} = \left(1 - x_p\right) \frac{A_k}{(1-\mathrm{LOI_k})\times 0.718} \quad (1)$$

Table 3. Estimated oxide chemistry of the pumice: kaolin blends (wt%)

Estimate (wt%)	25:75	50:50	75:25
SiO_2	56.2	60.0	63.8
Al_2O_3	29.4	24.6	19.8
Al_2O_3/SiO_2	0.52	0.41	0.31
$Na_2O + K_2O$	4.0	5.2	6.3
Total fluxes*	5.6	7.4	9.2
Upper-limit mullite, Equation (1)	38.9	25.9	13.0

F2O3 + CaO + MgO + Na2O + K2O. Estimates from the literature data in Table 2, not measurements on the tested batches.

Table 3 shows the chemical trade-off built into the design. Moving from 25 to 75 wt% pumice lowers the Al_2O_3/SiO_2 ratio from about 0.52 to 0.31, raises the total flux content from about 5.6 to 9.2 wt%, and cuts the upper-limit mullite from about 39 to 13 wt%. More glass and less mullite would be expected at high pumice content, which should favour bonding at 1200 °C but lower the softening temperature under load. These expectations are revisited in Sections 3.4, 3.6 and 3.7.

2.2. Experimental Design

Two factors were studied, each at three levels: the pumice: kaolin mass ratio (25:75, 50:50 and 75:25) and the pumice particle size (75, 150 and 300 µm). A Taguchi L9(3^4) orthogonal array was used because it gives a balanced nine-run design in which every level of one factor appears three times with every level of the other [34]. The array can hold four three-level factors, but only two variables were changed deliberately; the two unused columns were left empty, and their four degrees of freedom form the residual term in the ANOVA. Firing temperature was not a factor.

All specimens were fired at 1200 °C, and the temperatures of 800, 1000 and 1200 °C that appear later are nominal test temperatures for the thermal properties, not alternative firing conditions. Table 4 gives the formulation matrix. In the sample codes, the letter gives the particle size (A = 75 µm, B = 150 µm, C = 300 µm) and the number gives the pumice content (1 = 25 wt%, 2 = 50 wt%, 3 = 75 wt%). Two runs, B3 and C1, were later excluded from the analyses of porosity and bulk density (Sections 2.5 and 3.1).

Table 4. Taguchi L9 formulation matrix

Run	Code	Pumice (wt%)	Kaolin (wt%)	Pumice size (µm)
1	A1	25	75	75
2	A2	50	50	75
3	A3	75	25	75
4	B1	25	75	150
5	B2	50	50	150
6	B3	75	25	150
7	C1	25	75	300
8	C2	50	50	300
9	C3	75	25	300

2.3. Sample Preparation

Each batch was weighed according to Table 4, mixed dry and then wetted until it could be formed. Steel moulds on a hydraulic press were used to shape cylinders (35 mm diameter, 35 mm high), bars (150 mm long, 25 mm wide), prisms with a 20 × 10 mm cross-section and cones (57.20 mm high, 20.26 mm base). After 48 h of indoor drying, the specimens were fired in a gas kiln: the temperature was raised to 450 °C over 4 h so that water escaped slowly, then increased to 1200 °C and held for 1 h, after which the kiln was left closed to cool. Reliable values for the mixing water, mixing time and pressing pressure are not available in the laboratory records. They are not estimated here; their absence is listed as a limitation in Section 3.10 because they influence green density and fired porosity.

2.4. Property Evaluation

Table 5 lists the property tests, the standards followed, and the specimen geometry used for each test.

Table 5. Property tests, standards and specimen geometry

Property	Method and standard	Specimen
Apparent porosity, water absorption, apparent specific gravity, bulk density	Boiling-water Archimedes method, ASTM C20 [40]	Cylinder, 35 × 35 mm
Flexural strength, untreated and after thermal-shock treatment	Three-point bending on a universal testing machine, ASTM C1161 [41]	Bar, 150 × 25 mm
Pyrometric Cone Equivalent (PCE)	Orton cones, ASTM C24 [42]	Cone, 57.20 × 20.26 mm
Mean heat capacity from nominal 800, 1000 and 1200 °C	Drop calorimetry (method of mixtures)	Prism, 20 × 10 mm
Apparent thermal conductivity at nominal 800, 1000 and 1200 °C	Steady-state bar (Searle-type) method	Prism, 20 × 10 mm

In the Archimedes test, D is the dry mass, W the saturated mass and S the mass suspended in water. The apparent porosity P, water absorption A, bulk density B and apparent specific gravity T follow from Equations (2) to (5), with ρ_w the density of water [40].

$$P = \frac{W-D}{W-S} \times 100 \tag{2}$$

$$A = \frac{W-D}{D} \times 100 \tag{3}$$

$$B = \frac{D}{W-S}\rho_w \tag{4}$$

$$T = \frac{D}{D-S} \tag{5}$$

Flexural strength σ was obtained from the fracture load F, support span L, specimen width b and depth d with Equation (6). The as-fired (untreated) bars were tested in three-point bending without further treatment, and this is the strength used in the optimisation. A second set of bars was tested after a laboratory thermal-shock treatment, and a separate record gave percentage strength losses after repeated thermal-shock cycles. For neither procedure do the laboratory records state the temperature interval, the quench medium or the number of cycles, and the reference strength used to calculate the cyclic losses is not identified. Because the thermal-shock response of ceramics depends strongly on these parameters [43], the treated strengths are reported in Table 7 for completeness only and are not used in the optimisation, and the cyclic strength-loss data shown as Figure 1 in the previous version have been withdrawn.

$$\sigma = \frac{3FL}{2bd^2} \tag{6}$$

Heat capacity was measured by drop calorimetry. A specimen of mass m_s was heated to the nominal temperature T_s and dropped into a calorimeter holding water of mass m_w, specific heat c_w and initial temperature T_w, and the equilibrium temperature T_f was read. As Equation (7) shows, this method gives the mean specific heat of the specimen over the interval from T_f to T_s, not the specific heat at T_s; C_c is the heat capacity of the calorimeter vessel.

The calorimeter heat capacity was not determined, and the values in Table 8 were evaluated with $C_c = 0$. This omission and the heat lost while the hot specimen is transferred both lead to underestimated values, and the transfer loss grows with T_s. For thermal conductivity, a steady-state bar (Searle-type) arrangement was used, in which the steady heat flow Q through a bar of cross-section A_c and the temperature difference $T_1 - T_2$ over a gauge length L_b give k through Equation (8). The specimen length, thermocouple positions, method of heat-flow measurement, calibration against a reference material and heat-loss corrections are not

documented in the laboratory records, and it cannot be established whether 800, 1000 and 1200 °C denote the furnace set-point or the mean specimen temperature. The conductivities are therefore reported as apparent values at nominal temperatures; they are suitable for comparing the formulations with one another but only indicative in absolute terms.

$$\overline{c}_{\mathrm{s}} = \frac{(m_{\mathrm{w}}c_{\mathrm{w}}+C_{\mathrm{c}})(T_{\mathrm{f}}-T_{\mathrm{w}})}{m_{\mathrm{s}}(T_{\mathrm{s}}-T_{\mathrm{f}})} \tag{7}$$

$$k = \frac{QL_{\mathrm{b}}}{A_{\mathrm{c}}(T_1-T_2)} \tag{8}$$

Refractoriness was assessed with Orton pyrometric cones following ASTM C24 [42]. Test cones of each formulation were heated in the kiln to 1200 °C together with reference cones 05, 02 and 1, whose nominal chart equivalents are 1062, 1148 and 1184 °C. The heating rate of this test and the bending state of each reference cone at the end of the run were not recorded. Because cone equivalents depend on heating rate, the result is reported as the observation that no test cone deformed up to a kiln temperature of 1200 °C, and no cone number is assigned. The design was not replicated at the formulation level, so each tabulated value is a single formulation-level result, and no standard deviations are reported; Section 3.10 discusses the consequences.

2.5. Statistical Analysis and Multi-Response Optimisation

Four responses were used for optimisation: bulk density, apparent porosity, as-fired flexural strength and apparent thermal conductivity at a nominal 1000 °C. As-fired strength replaces the thermal-shock-treated strength of the previous version because the treatment parameters are not documented (Section 2.4). Water absorption was left out because, by Equations (2) to (4), it equals P/B and carries no independent information. Formulations B3 and C1 failed the apparent specific gravity check of Section 3.1. Because the suspected error in the suspended mass affects both porosity and bulk density, these two runs were excluded from every analysis that uses either property, including the correlations, S/N response tables, ANOVA and GRA; their strength and conductivity values, which do not depend on the Archimedes measurement, were retained where those responses are analysed on their own. Bulk density was treated as smaller-the-better because ASTM C155 sets a maximum bulk density for insulating firebrick [39]; porosity and strength were larger-the-better, and conductivity smaller-the-better. The S/N ratios were calculated with Equations (9) and (10) [34], with porosity entered as a fraction.

$$S/N = -10\log_{10}\left[\frac{1}{n}\sum_{i=1}^{n}\frac{1}{y_i^2}\right] \tag{9}$$

$$S/N = -10\log_{10}\left[\frac{1}{n}\sum_{i=1}^{n}y_i^2\right] \tag{10}$$

Main-effects ANOVA was carried out at $\alpha = 0.05$ [35]. For the complete nine-run responses (as-fired strength and conductivity), the sum of squares of factor j and its percentage contribution follow from Equations (11) and (12), where $\bar{y}_{j,l}$ is the mean response at level l of factor j, $\bar{y}$ is the grand mean, and SS_{T} is the total sum of squares; each factor then has 2 degrees of freedom and the residual 4. With B3 and C1 removed, the design is no longer balanced, so bulk density, porosity and the grey relational grade were analysed by least-squares fitting of the additive model with Type II sums of squares, which leaves 2 residual degrees of freedom; contributions in this case need not add to 100%. In both cases, the runs were not replicated, so the residual combines experimental error with any pumice content × particle size interaction, and the F-tests have low power.

$$SS_j = 3\sum_{l=1}^{3}\left(\overline{y}_{j,l}-\overline{y}\right)^2 \tag{11}$$

$$C_j = \frac{SS_j}{SS_{\mathrm{T}}}\times 100\% \tag{12}$$

For GRA [36], each response $y_i(k)$ was normalised to $x_i(k)$ with Equation (13) for larger-the-better responses and Equation (14) for smaller-the-better responses. The deviation sequence is $\Delta_{0i}(k) = 1 - x_i(k)$. The grey relational coefficient $\xi_i(k)$ was obtained from Equation (15) with a distinguishing coefficient $\zeta = 0.5$, and the Grey Relational Grade (GRG) γ_i was taken as the equally weighted mean over the $m = 4$ responses, Equation (16).

$$x_i(k) = \frac{y_i(k)-\min y(k)}{\max y(k)-\min y(k)} \tag{13}$$

$$x_i(k) = \frac{\max y(k)-y_i(k)}{\max y(k)-\min y(k)} \tag{14}$$

$$\xi_i(k) = \frac{\Delta_{\min}+\zeta\Delta_{\max}}{\Delta_{0i}(k)+\zeta\Delta_{\max}} \tag{15}$$

$$\gamma_i = \frac{1}{m}\sum_{k=1}^{m}\xi_i(k) \tag{16}$$

Factor-level mean response analysis was then applied to the GRG. Because the retained runs are unbalanced, the level means were taken as least-squares marginal means of the additive model, which correct for the missing cells. The best level of each factor identifies the predicted optimum, and the grade at that point follows from Equation (17), where γ_{m} is the grand mean GRG and $\bar{\gamma}_{j,\mathrm{opt}}$ is the mean GRG at the best level of factor j [34]. Every retained run, including any run at the predicted optimum, is part of the data used to fit the model. Agreement between predicted and measured grades is, therefore, an internal fit check and not an independent confirmation.

$$\hat{\gamma} = \gamma_{\mathrm{m}} + \sum_{j=1}^{2}\left(\overline{\gamma}_{j,\mathrm{opt}}-\gamma_{\mathrm{m}}\right) \tag{17}$$

Because a grey relational ranking can depend on analyst choices [38], thirteen scenarios were examined: ζ from 0.1 to 1.0; insulation-weighted and strength-weighted schemes; conductivity at 800 or 1200 °C instead of 1000 °C; bulk density treated as larger-the-better; treated instead of as-fired strength; all nine runs with strength and conductivity only; and all nine runs with the values as reported. All calculations were performed in Python with NumPy and SciPy, and *p*-values were taken from the *F* distribution.

2.6. Derived Thermal Parameters and Benchmarking Method

Derived quantities were used to test the internal consistency of the data. Combining Equations (2) to (5) gives the identities of Equation (18). Apparent specific gravity excludes open pores but includes closed pores, so T can be lower than the true density of the solid but cannot exceed it [40].

An apparent solid-phase conductivity k_s was back-calculated from the measured k and P with the Maxwell-Eucken relation for pores of negligible conductivity, Equation (19) [30]; because apparent porosity counts open pores only, this k_s is a lower estimate.

$$A = \frac{P}{B},\ T = \frac{B}{1-P} \tag{18}$$

$$k_s = k\frac{1+P/2}{1-P} \tag{19}$$

For benchmarking, bulk density was compared with the group limits of ASTM C155 [39], and density, strength and conductivity with a commercial insulating firebrick data sheet [44] and with published clay composites [14, 22, 23]. To show what the conductivity values imply for a lining, a 230 mm single-layer wall with a hot face at 1000 °C and a cold face at 100 °C was assumed, and the steady heat flux q and the lining mass per unit area m_A were calculated with Equation (20). Heat storage was compared only in relative terms, as m_A divided by that of a dense reference brick, which assumes a similar mean specific heat for all aluminosilicate materials; the measured heat capacities were not used, for the reasons given above.

$$q = \frac{k\Delta T}{L},\ m_A = \rho L \tag{20}$$

3. Results and Discussion

3.1. Physical Properties

Table 6. Physical properties of the fired composites

Code	*P* (%)	*A* (%)	*T*	*B* (g/cm³)
A1	43.3	28.89	2.65	1.50
A2	24.2	12.31	2.60	1.97
A3	34.3	19.05	2.74	1.80
B1	33.3	23.08	2.17	1.44
B2	46.9	31.91	2.76	1.47
B3*	71.4	40.00	6.25	1.79
C1*	58.8	40.00	3.57	1.47
C2	32.5	20.97	2.30	1.55
C3	33.3	16.67	3.00	2.00

P = apparent porosity; A = water absorption; T = apparent specific gravity; B = bulk density. B3 and C1 failed the apparent specific gravity check (Section 3.1); their P, A and B values are shown as measured but are excluded from all analyses.*

Table 6 lists the physical properties. Among the seven formulations that passed the consistency check, apparent porosity ranged from 24.2% (A2: 50 wt% pumice, 75 µm) to 46.9% (B2: 50 wt% pumice, 150 µm), water absorption from 12.31% (A2) to 31.91% (B2), and bulk density from 1.44 g/cm³ (B1) to 2.00 g/cm³ (C3). Bulk density rose with pumice content, averaging 1.47, 1.66 and 1.90 g/cm³ for 25, 50 and 75 wt% pumice over the retained runs. A denser body at higher pumice content runs against the usual role of pumice as a lightweight additive. One possible explanation is that the more fluxed bodies (Table 3) develop more glass at 1200 °C, which flows into the voids of the kaolin skeleton, and that milling to 75 to 300 µm opens much of the original vesicle structure. Both ideas remain hypotheses until they are checked by microscopy.

Porosity did not follow either factor in a simple way. At 25 wt% pumice, it fell from 43.3% (A1) to 33.3% (B1); at 50 wt% it rose from 24.2% (A2) to 46.9% (B2) and then fell to 32.5% (C2). The previous version treated the step from B1 to C1 (58.8%) as the clearest particle-size effect, but the porosity of C1 failed the consistency check described below, and that comparison has been withdrawn. The remaining non-monotonic pattern suggests that particle size and pumice content may interact; the main-effects design cannot separate such an interaction from error, so it is noted as a possibility rather than claimed (Section 2.5).

Two consistency checks were applied with Equation (18). The first confirms that $A = P/B$ holds for all nine formulations to within rounding; it also shows that the identical water absorption of B3 and C1 (40.00%) is an arithmetic coincidence, since 0.714/1.79 and 0.588/1.47 both round to 0.40. The second check uses the fact that T includes closed pores and therefore cannot exceed the true density of the solid. No measured phase composition is available for these bodies, so no exact limit can be set. Even so, the densest phase that can plausibly form, mullite, has a true density of about 3.2 g/cm³ [25], and silica glass, quartz and cristobalite are lighter. B3 (6.25) and C1 (3.57) exceed this value and are physically implausible. C3 (3.00) lies below it; the previous version wrongly grouped C3 with the anomalous specimens. B1 has the lowest value (2.17), which closed porosity can explain, and which does not, by itself, indicate a measurement error. Because T depends only on the dry and suspended masses, the B3 and C1 results most likely reflect an overestimated

suspended mass, for example from incomplete immersion or contact with the support, and such an error inflates both *P* and *B*. Remeasurement of these two formulations could not be completed within the revision period, so both runs were excluded from all analyses that use porosity or bulk density (Section 2.5). The water absorption of 12 to 40% also has a practical consequence. Open pores that can take up this much water will change the effective thermal conductivity if the lining is exposed to damp storage, rain or condensation before firing. The conductivities reported here are dry-state values and should not be read as service values under wet conditions [32, 45].

3.2. Mechanical Properties

Table 7. Flexural strength of untreated and thermally shocked specimens

Code	Untreated (MPa)	After thermal-shock treatment (MPa)	Change (%)
A1	0.25	0.62	+148.0
A2	0.95	1.15	+21.1
A3	0.88	0.98	+11.4
B1	0.72	0.86	+19.4
B2	0.42	0.58	+38.1
B3	0.55	0.68	+23.6
C1	0.34	0.38	+11.8
C2	0.46	0.45	−2.2
C3	0.18	0.19	+5.6

Change = (treated − untreated)/untreated × 100. Treated values follow a laboratory thermal-shock treatment whose parameters were not documented (Section 2.4); they are reported for completeness and are not used in the optimisation.

Table 7 lists the flexural strengths. As-fired strength ranged from 0.18 MPa (C3) to 0.95 MPa (A2). Mean as-fired strength was 0.69, 0.56 and 0.33 MPa for 75, 150 and 300 µm pumice, and 0.44, 0.61 and 0.54 MPa for 25, 50 and 75 wt% pumice. Particle size made the larger contribution in the ANOVA (35.2%), but neither factor was significant ($p = 0.38$ for particle size and 0.78 for pumice content), and 57.1% of the variation remained in the residual (Section 3.5.3). Lower strength with coarse pumice would be consistent with coarse grains acting as weakly bonded inclusions, but the present data do not establish this, and no microscopy is available to test it.

The treated bars recorded higher strength than the untreated bars in eight of the nine formulations, including a 148% increase for A1. The previous version attributed this to viscous flow of the glassy phase healing surface flaws, and that explanation has been removed. Without repeat specimens, uncertainty estimates, or a documented treatment, the differences cannot be separated from specimen-to-specimen scatter, so the data do not establish thermal-shock strengthening. The percentage strength losses after repeated cycling, shown as Figure 1 in the previous version, have been withdrawn for the same reason and because the reference strength used to calculate them cannot be identified; those values could not be reconciled with Table 7. Thermal-shock behaviour will be reassessed with a standard water-quench procedure, a stated temperature difference and cycle count, and at least three specimens per formulation.

3.3. Thermal Properties

Table 8. Mean heat capacity from drop calorimetry, between the calorimeter equilibrium temperature and the nominal temperature (J/g·K)

Code	From 800 °C	From 1000 °C	From 1200 °C
A1	1.45	1.75	1.08
A2	1.27	1.64	0.97
A3	1.20	1.57	0.85
B1	1.14	1.51	0.95
B2	1.00	1.43	0.85
B3	0.90	1.38	0.74
C1	0.85	1.22	0.81
C2	0.81	1.20	0.72
C3	0.78	1.14	0.61

Table 8 gives the mean heat capacities. Each value is an average over the interval from the calorimeter equilibrium temperature, close to room temperature, up to the nominal temperature, and not the specific heat at the nominal temperature. Within each column, the values fell as pumice content and particle size increased, and the ranking of the formulations was consistent at 800 and 1000 °C, while at 1200 °C, the ranking changed with B1 (0.95 J/g.k) exhibiting a higher mean heat capacity than A3 (0.85 J/g.k). The absolute values are less secure. A mean heat capacity taken over a wider interval should rise steadily with the upper temperature, yet the values rise from 800 to 1000 °C and then fall by 34 to 47% from 1000 to 1200 °C. This pattern is consistent with the two systematic errors described in Section 2.4, the neglected calorimeter heat capacity and transfer losses that grow with temperature. The heat-capacity data are therefore treated as comparative only. They are not used in any thermal calculation in this revision, and differential scanning calorimetry is needed before absolute values can be reported.

Table 9. Apparent thermal conductivity at the nominal test temperatures (W/m·K)

Code	800 °C	1000 °C	1200 °C	Fall 800 to 1200 °C (%)
A1	1.47	1.33	1.07	27.2
A2	1.82	1.38	1.12	38.5
A3	2.02	1.41	1.14	43.6
B1	2.33	1.44	1.18	49.4
B2	2.34	1.48	1.23	47.4
B3	2.50	1.57	1.29	48.4
C1	2.67	1.62	1.32	50.6
C2	2.91	1.59	1.36	53.3
C3	3.28	1.68	1.39	57.6

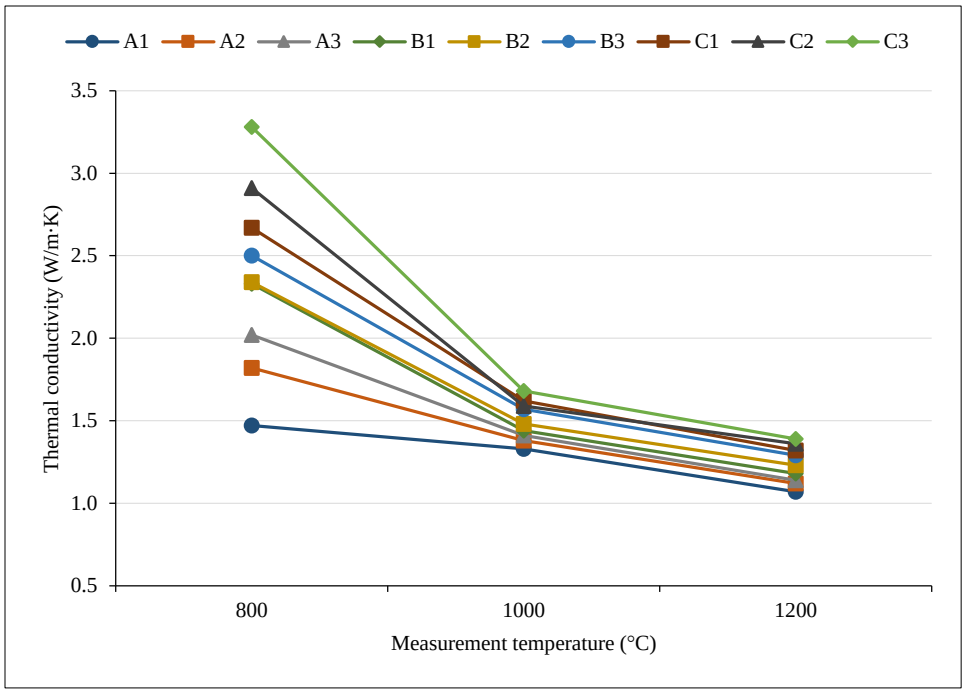


Fig. 1 Apparent thermal conductivity of the nine formulations at the nominal test temperatures of 800, 1000 and 1200 °C (all specimens fired at 1200°C)

Table 9 and Figure 1 show that the apparent conductivity fell with nominal test temperature for every formulation, from 1.47 to 3.28 W/m·K at 800 °C, to 1.33 to 1.68 W/m·K at 1000 °C and 1.07 to 1.39 W/m·K at 1200 °C, a reduction of 27% (A1) to 58% (C3) between 800 and 1200 °C. Reductions of this size need independent confirmation: because the apparatus details and heat-loss corrections are not documented (Section 2.4), part of the change may come from the measurement rather than the material.

The previous version took the direction of the change as evidence of conduction through crystalline phases. Phonon scattering does reduce the conductivity of crystalline oxides as temperature rises [30, 33], but the direction of a trend alone does not establish which phases conduct, and that interpretation has been withdrawn.

At a nominal 1000 °C, particle size had the largest effect on conductivity: the means were 1.37, 1.50 and 1.63 W/m·K for 75, 150 and 300 µm (85.8% contribution, p = 0.0008), against 1.46, 1.48 and 1.55 W/m·K for 25, 50 and 75 wt% pumice (11.6%, p = 0.032). Over the seven retained runs, conductivity was almost unrelated to porosity (r = −0.12), so the porosity data alone do not explain the particle-size effect.

One possibility is that fine pumice reacts more completely with the kaolin and leaves more glass of low intrinsic conductivity, but this remains a hypothesis. Table 10 lists the apparent solid conductivity from Equation (19). It lies between 2.0 and 3.4 W/m·K for the seven retained formulations and rises to 5.09 W/m·K for C1 and 7.45 W/m·K for B3; the last two values are improbable for an aluminosilicate body and support the exclusion of these runs.

Table 10. Consistency indicators: apparent specific gravity and apparent solid conductivity at a nominal 1000 °C

Code	*T*	k_s, Equation (19) (W/m·K)	Status
A1	2.65	2.85	Retained
A2	2.60	2.04	Retained
A3	2.74	2.51	Retained
B1	2.17	2.52	Retained
B2	2.76	3.44	Retained
B3	6.25	7.45	Excluded
C1	3.57	5.09	Excluded
C2	2.30	2.74	Retained
C3	3.00	2.94	Retained

T from Table 6; ks from Equation (19) with the measured k at a nominal 1000 °C and P. A value of T above about 3.2 g/cm3, the true density of mullite [25], is physically implausible.

The thermal diffusivity and volumetric heat capacity reported in the previous version depended on the drop-calorimetry results and have been removed. Once conductivity and heat capacity have been confirmed by laser-flash and calorimetric methods, these properties can serve as inputs to transient heat-transfer models of a furnace wall, of the kind now applied to insulated building envelopes and foundations [45, 46].

3.4. Refractoriness

No test cone deformed or bent before the kiln reached 1200 °C, the highest temperature of the test. On the nominal Orton chart, cone 1 corresponds to 1184 °C, so the formulations would have a pyrometric cone equivalent above that value [42]. Because the heating rate and the bending of the reference cones were not recorded, and cone equivalents depend on heating rate, this figure is indicative and is reported as a lower bound rather than as a cone number; the true softening point was not reached. Dense, kaolin-rich crucible bodies made from Ikere clay have an estimated refractoriness of 1680 to 1717 °C [10]. The present composites contain considerably more flux, about 5.6 to 9.2 wt% according to Table 3, so their softening point is expected to be lower and to fall with pumice content. The observation shows that the composites remain shape-stable without load up to 1200 °C. It does not set a service temperature and says nothing about behaviour under load (Section 3.7).

3.5. Multi-Objective Optimisation

3.5.1. Correlation between Responses

Table 11. Pearson correlation coefficients between responses

	P	A	B	σ_u	k_{1000}
P	1.00				
A	0.95	1.00			
B	−0.64	−0.84	1.00		
σ_u	−0.59	−0.48	0.20	1.00	
k_{1000}	−0.12	−0.22	0.27	−0.52	1.00

Correlations involving P, A or B use the seven retained runs (n = 7; $|r| \geq 0.75$ significant at $p < 0.05$); the others use all nine runs (n = 9; $|r| \geq 0.67$). σu = as-fired flexural strength; k1000 = apparent conductivity at a nominal 1000 °C.

Table 11 gives the correlations. Porosity and water absorption are almost the same variable (r = 0.95), which justifies omitting water absorption from the optimisation. With B3 and C1 removed, porosity and bulk density show the expected negative relation (r = −0.64), and water absorption falls significantly with bulk density (r = −0.84, p = 0.018); in the previous version, which kept the doubtful runs, the porosity-density correlation was only −0.26.

As-fired strength tends to fall as porosity rises (r = −0.59) and as conductivity rises (r = −0.52), but neither relation is significant at this sample size.

The previous version linked conductivity strongly to treated strength and to specific heat; both of those responses have been removed from the analysis, and the statements withdrawn. Because density, porosity, strength and conductivity do not favour the same formulations, a multi-response method is still required.

3.5.2. Signal-to-Noise Ratio Analysis

Table 12. S/N ratios of the four optimisation responses (dB)

Code	B (S)	P (L)	σ_u (L)	k_{1000} (S)
A1	−3.52	−7.27	−12.04	−2.48
A2	−5.89	−12.32	−0.45	−2.80
A3	−5.11	−9.29	−1.11	−2.98
B1	−3.17	−9.55	−2.85	−3.17
B2	−3.35	−6.58	−7.54	−3.41
B3	excl.	excl.	−5.19	−3.92
C1	excl.	excl.	−9.37	−4.19
C2	−3.81	−9.76	−6.74	−4.03
C3	−6.02	−9.55	−14.89	−4.51

S = smaller-the-better; L = larger-the-better. Porosity entered as a fraction; σu = as-fired strength. excl. = excluded run (Section 3.1).

Table 12 lists the S/N ratios; a larger S/N is better in every column. The porosity column is larger-the-better, which corrects a labelling error in the first submission. The strength column now uses as-fired strength, for which A2 has the best ratio (−0.45 dB) and C3 the worst (−14.89 dB).

For conductivity, A1 has the best ratio (−2.48 dB) and C3 the worst (−4.51 dB), corresponding to the lowest and highest conductivities. Bulk density is treated as smaller-the-better, in line with the aim of an insulating lining. The density and porosity ratios of B3 and C1 are not shown because those runs were excluded.

Table 13. Mean S/N response by factor level (dB)

Level	B		P		σ_u		k_{1000}	
	Pumice	Size	Pumice	Size	Pumice	Size	Pumice	Size
1	−3.40	−4.84	−8.62	−9.63	−8.09	−4.53	−3.28	−2.75
2	−4.35	−3.72	−9.55	−8.00	−4.91	−5.19	−3.41	−3.50
3	−5.25	−4.45	−8.91	−9.45	−7.07	−10.34	−3.80	−4.24
Delta	1.85	1.12	0.93	1.62	3.18	5.80	0.52	1.49
Rank	1	2	2	1	2	1	2	1

Pumice levels 1, 2, 3 = 25, 50, 75 wt%; size levels 1, 2, 3 = 75, 150, 300 µm. For B and P, least-squares marginal means of the additive model from the seven retained runs; for σu and k1000, arithmetic means over nine runs. The best level in each column has the highest mean S/N.

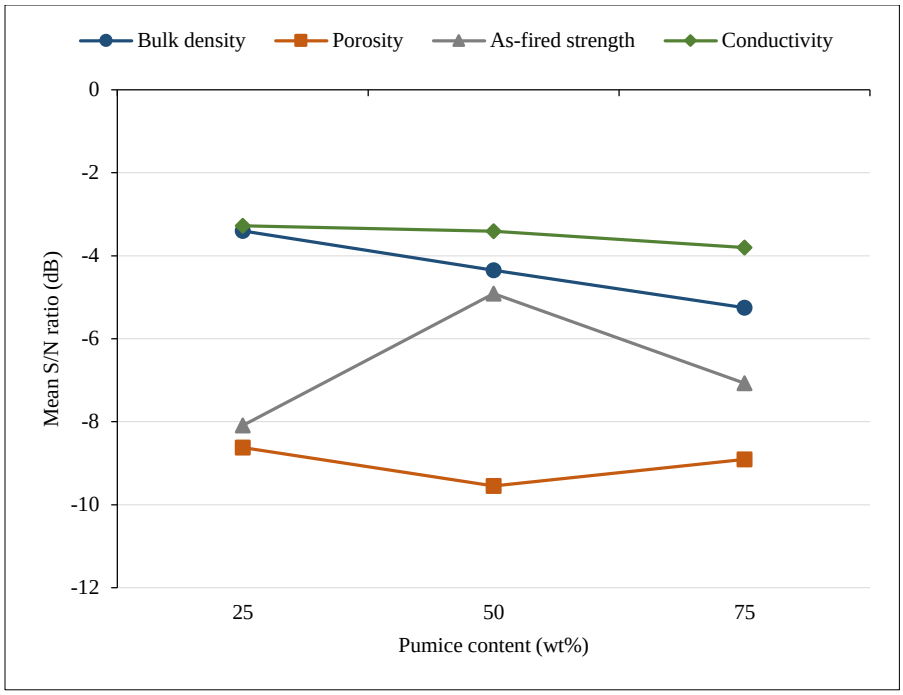


Fig. 2 Main effects of pumice content on the mean S/N ratio of the four responses (density and porosity from the seven retained runs)

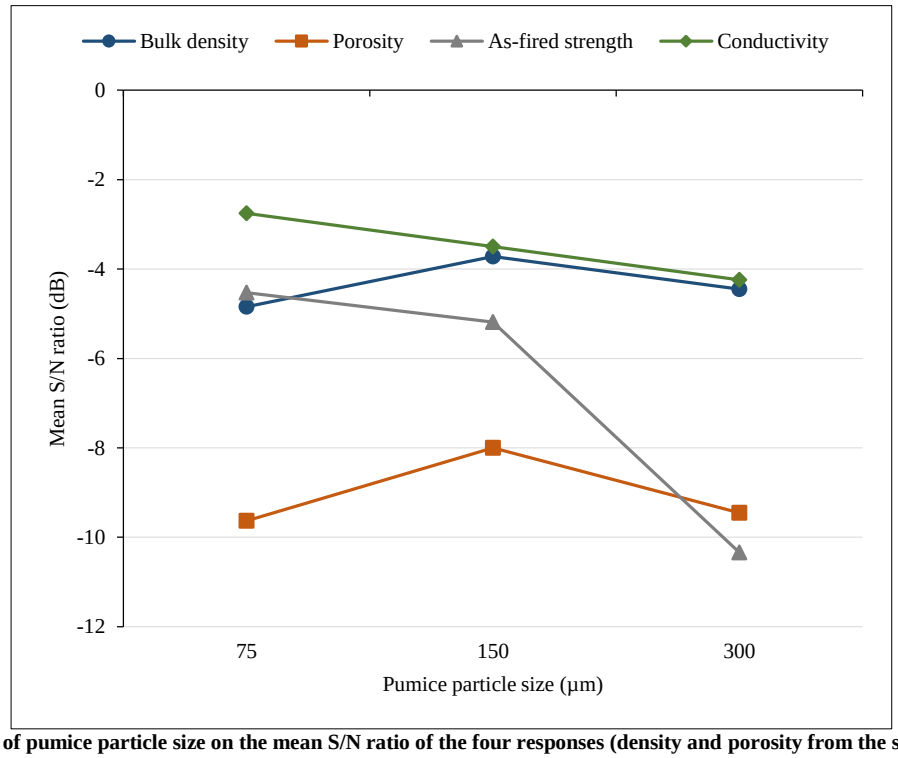


Fig. 3 Main effects of pumice particle size on the mean S/N ratio of the four responses (density and porosity from the seven retained runs)

Table 13 and Figures 2 and 3 give the mean S/N at each factor level. Low density favours 25 wt% pumice and 150 µm; high porosity favours 150 µm and, to a lesser extent, 25 wt% pumice; high as-fired strength favours 75 µm and 50 wt% pumice; and low conductivity favours 75 µm and 25 wt% pumice.

Particle size has the larger delta for porosity, strength and conductivity, and pumice content for bulk density. The largest effect in the table is that of particle size on as-fired strength (delta 5.80 dB), driven mainly by the low strength at 300 µm. No single combination is best for all four responses, which is the situation GRA is designed to resolve.

3.5.3. Analysis of Variance

Table 14 gives the ANOVA. At $\alpha = 0.05$, both factors were significant for conductivity at a nominal 1000 °C (particle size 85.8%, $p = 0.0008$; pumice content 11.6%, $p = 0.032$). Neither factor was significant for bulk density (pumice content 27.6%, $p = 0.55$), porosity (particle size 13.8%, $p = 0.85$) or as-fired strength (particle size 35.2%, $p = 0.38$). For density and porosity only two residual degrees of freedom remain once B3 and C1 are excluded, so these tests can detect only very large effects; the non-significant results mean that the effects are unresolved, not that they are absent. The specific-heat ANOVA of the previous version has been removed together with the heat-capacity data from the analysis.

Table 14. Main-effects ANOVA of the measured responses

Response	Source	DF	SS	MS	*F*	*p*	*C* (%)
Bulk density (7 runs)	Pumice content	2	0.09721	0.04860	0.83	0.5478	27.63
	Particle size	2	0.04831	0.02415	0.41	0.7091	13.73
	Residual	2	0.1178	0.05888			33.48
	Total	6	0.3518				
Apparent porosity (7 runs)	Pumice content	2	7.7467	3.8733	0.03	0.9719	2.29
	Particle size	2	46.69	23.34	0.17	0.8515	13.79
	Residual	2	267.66	133.83			79.06
	Total	6	338.54				
As-fired flexural strength (9 runs)	Pumice content	2	0.04542	0.02271	0.27	0.7763	7.71
	Particle size	2	0.2074	0.1037	1.23	0.3829	35.18
	Residual	4	0.3366	0.08414			57.11
	Total	8	0.5894				
Apparent thermal conductivity, nominal 1000 °C (9 runs)	Pumice content	2	0.01340	0.00670	9.14	0.0323	11.63
	Particle size	2	0.09887	0.04943	67.41	0.0008	85.82
	Residual	4	0.00293	0.000733			2.55
	Total	8	0.1152				

DF = degrees of freedom; SS = sum of squares; MS = mean square; C = percentage contribution. For the seven-run responses (unbalanced), Type II sums of squares are used, and contributions need not sum to 100%. The residual includes any pumice × size interaction.

3.5.4. Grey Relational Analysis

Table 15 sets out every step of the GRA for the seven retained runs so that the ranking can be reproduced. A1 (25 wt% pumice, 75 µm) has the highest grade (0.7344), followed by B2 (0.7156) and B1 (0.6737); C3 is last (0.3637). A1 combines the lowest conductivity with low density and moderate porosity, but it has the second-lowest as-fired strength; B2 has high porosity and low density with moderate strength and conductivity. The grades differ from those of the previous version for two reasons: as-fired strength replaces treated strength, and B3 and C1 are excluded. The leading formulation is unchanged.

Table 15. Grey relational analysis of the seven retained runs: normalised values, coefficients, grades and ranks (ζ = 0.5)

Code	Normalised value $x_i(k)$				Grey relational coefficient $\xi_i(k)$				GRG	Rank
	B	*P*	σ_u	*k*	*B*	*P*	σ_u	*k*		
A1	0.8929	0.8414	0.0909	1.0000	0.8235	0.7592	0.3548	1.0000	0.7344	1
A2	0.0536	0.0000	1.0000	0.8571	0.3457	0.3333	1.0000	0.7778	0.6142	4
A3	0.3571	0.4449	0.9091	0.7714	0.4375	0.4739	0.8462	0.6863	0.6110	5
B1	1.0000	0.4009	0.7013	0.6857	1.0000	0.4549	0.6260	0.6140	0.6737	3
B2	0.9464	1.0000	0.3117	0.5714	0.9032	1.0000	0.4208	0.5385	0.7156	2
C2	0.8036	0.3656	0.3636	0.2571	0.7179	0.4408	0.4400	0.4023	0.5003	6
C3	0.0000	0.4009	0.0000	0.0000	0.3333	0.4549	0.3333	0.3333	0.3637	7

Directions: B smaller-the-better; P and σu (as-fired strength) larger-the-better; k at a nominal 1000 °C smaller-the-better. Equal weights. B3 and C1 excluded (Section 3.1).

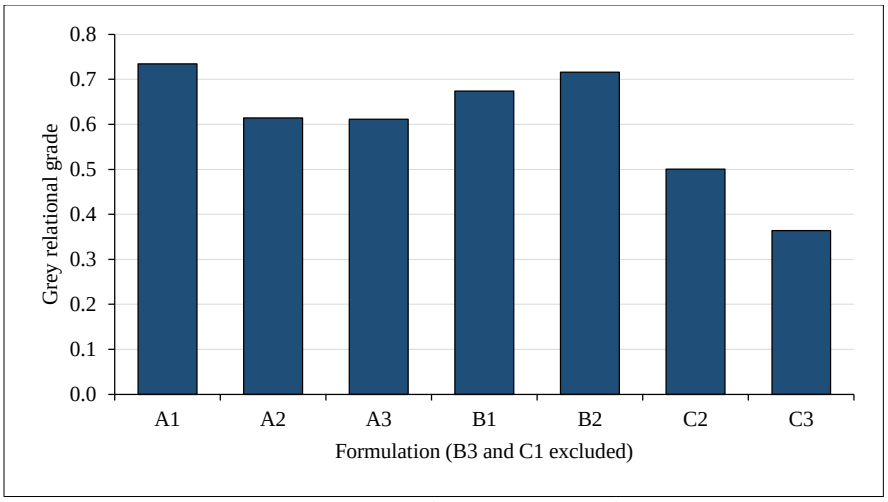


Fig. 4 Grey relational grade of the seven retained formulations

3.5.5. Factor-Level Mean Response Analysis of the GRG

Table 16 and Figure 5 give the factor-level analysis of the GRG. The least-squares level means fall with pumice content (0.6368, 0.6100 and 0.5230), while for particle size, the 75 and 150 µm levels are almost equal (0.6532 and 0.6612), and 300 µm is clearly lower (0.4554).

The nominal best combination, 25 wt% pumice with 150 µm, corresponds to B1, for which Equation (17) predicts 0.7081 against a measured 0.6737; the model fits A1 at 0.7001 against a measured 0.7344. The difference between the 75 and 150 µm levels (0.008) is much smaller than the residual standard deviation of the model (about 0.067), so the data identify a preferred region, 25 wt% pumice with particles of 75 to 150 µm, rather than a single point; within that region, A1 has the highest measured grade. These comparisons are internal fit checks because A1 and B1 are part of the data used to build the model, and neither factor was significant in the ANOVA of the GRG (particle size 45.4%, p = 0.16; pumice content 10.9%, p = 0.44). An independent, replicated confirmation run at 25 wt% pumice with 75 and 150 µm particles is therefore required before the optimum can be regarded as established.

Table 16. Least-squares mean GRG by factor level and ANOVA of the GRG (seven retained runs)

Factor	Level 1	Level 2	Level 3	Delta	Best level	*C* (%)	*p*
Pumice content	0.6368	0.6100	0.5230	0.1138	25 wt%	10.91	0.441
Particle size	0.6532	0.6612	0.4554	0.2058	150 µm*	45.42	0.159
Residual						8.61	

The 75 µm level is lower by only 0.008, well within the residual standard deviation (about 0.067). Type II ANOVA, 2 residual DF. Predicted GRG at 25 wt% and 150 µm (B1, Equation 17) = 0.7081, measured 0.6737; fitted GRG of A1 = 0.7001, measured 0.7344. These are internal fit checks, not independent confirmation

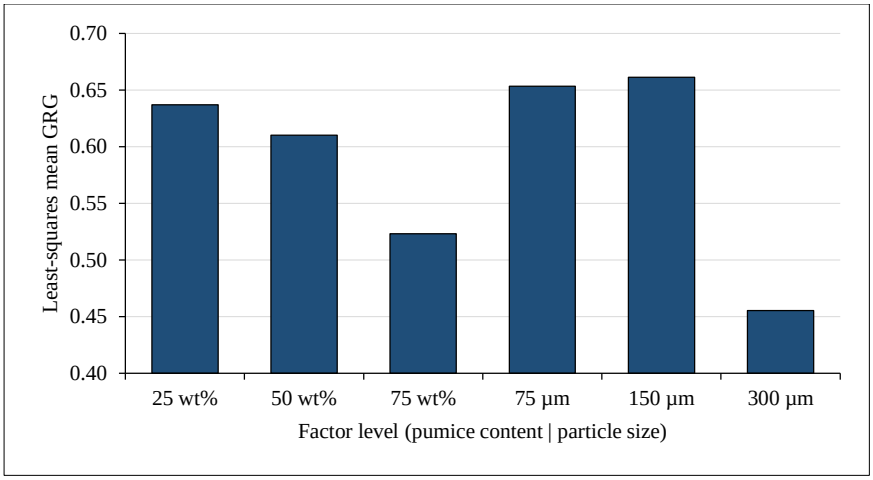


Fig. 5 Least-squares mean grey relational grade at each level of pumice content and particle size (seven retained runs)

3.5.6. Sensitivity of the Ranking

Table 17 shows that A1 ranked first in ten of the thirteen scenarios, including every value of ζ from 0.1 to 1.0, the insulation-weighted scheme, conductivity at 800 or 1200 °C, the use of treated instead of as-fired strength, and the analysis of all nine runs with the values as reported.

A2 moved to first place in the other three: when strength was given double weight, when bulk density was treated as larger-the-better, and when only strength and conductivity were used across all nine runs.

In each of those cases, densification and strength, rather than lightness, are rewarded. B2 or B1 occupied second place in most scenarios. On present evidence, A1 is the preferred formulation where low conductivity and low mass are the priority, and A2 (50 wt% pumice, 75 µm) where strength matters more, subject to the confirmation tests noted above.

Table 17. Sensitivity of the GRA ranking to analyst choices

Scenario	First	Second	Third	Rank of A1
ζ = 0.1, equal weights	A1 (0.492)	B2 (0.492)	B1 (0.409)	1
ζ = 0.3, equal weights	A1 (0.660)	B2 (0.641)	B1 (0.581)	1
ζ = 0.5, equal weights	A1 (0.734)	B2 (0.716)	B1 (0.674)	1
ζ = 0.7, equal weights	A1 (0.779)	B2 (0.763)	B1 (0.733)	1
ζ = 1.0, equal weights	A1 (0.823)	B2 (0.810)	B1 (0.789)	1
Insulation-weighted (P and k ×2)	A1 (0.783)	B2 (0.734)	B1 (0.627)	1
Strength-weighted (σ ×2)	A2 (0.691)	B1 (0.664)	A1 (0.658)	3
k at 800 °C instead of 1000 °C	A1 (0.734)	B2 (0.709)	B1 (0.648)	1
k at 1200 °C instead of 1000 °C	A1 (0.734)	B2 (0.706)	B1 (0.668)	1
Bulk density treated as larger-the-better	A2 (0.754)	A3 (0.647)	A1 (0.618)	3
Treated strength instead of as-fired strength	A1 (0.764)	B2 (0.725)	B1 (0.673)	1
All nine runs, strength and k only	A2 (0.889)	A3 (0.766)	A1 (0.677)	3
All nine runs, values as reported	A1 (0.659)	B1 (0.656)	A2 (0.614)	1

Values in brackets are GRGs. Unless stated, ζ = 0.5, equal weights, the seven retained runs and the four responses of Table 15.

3.6. Microstructural and Phase-Evolution Considerations

Scanning electron microscopy, energy-dispersive spectroscopy and XRD were not available within this experimental programme. The first submission described mullite formation, pore closure and microcracking as if they had been observed. Those statements have been removed, and the discussion below is limited to what published phase studies predict and to what the present bulk data can support.

When kaolin is heated, kaolinite loses its structural water between about 450 and 750 °C to form amorphous metakaolin; above about 950 °C, a spinel phase or primary mullite crystallises, and at 1200 °C, mullite coexists with silica-rich glass and, depending on time, cristobalite [10, 25, 26]. In clay bodies that contain alkali, the flux lowers the temperature at which liquid appears, and mullite grows from this liquid as fine needles [24]. Pumice supplies an alkali-rich glass that softens well below 1200 °C. Its finer fractions should therefore dissolve more completely into the kaolin-derived matrix, while coarse grains may survive as partly reacted inclusions surrounded by an interfacial zone.

Two observations in this study are compatible with that picture, although neither proves it. Bulk density increases with pumice content (Section 3.1), which would be expected if the more fluxed bodies develop more viscous glass. As-fired strength is lowest for the 300 µm particles (Section 3.2), which would be expected if coarse grains remain as partly reacted inclusions. The upper-limit mullite contents estimated in Table 3, about 39, 26 and 13 wt% for 25, 50 and 75 wt% pumice, indicate how quickly the potential crystalline fraction falls as pumice replaces kaolin. The temperature dependence of conductivity is no longer used as evidence for crystalline phases (Section 3.3). Quantitative XRD with Rietveld refinement, SEM of polished and fractured sections, and EDS mapping of the pumice-matrix interface are needed to test these interpretations.

3.7. Refractoriness under Load and High-Temperature Creep

Refractoriness under load and compressive creep describe how a refractory deforms under the weight of the lining at service temperature; neither was measured in this study. The relevant tests are the refractoriness-under-load test of ISO 1893 [47] and the creep test of ASTM C832 [48], and RUL testing can also provide the temperature-dependent elastic modulus of refractory ceramics [49].

The cone observation of Section 3.4 is a lower bound for unloaded softening and cannot be converted into a load-bearing limit, because deformation under load normally begins well below the unloaded softening temperature. The rise in estimated flux content from about 5.6 to 9.2 wt% between the 25 and 75 wt% pumice blends (Table 3) suggests that resistance to deformation under load will decrease with pumice content, and A1, with the lowest flux content and the

highest mullite potential, would be expected to perform best. No service temperature or load rating is proposed here; both must await RUL, creep and ASTM C210 reheat-change results [50].

3.8. Techno-Economic and Environmental Screening

A full cost-benefit analysis and Life-Cycle Assessment (LCA) could not be carried out with defensible inputs, because plant-scale data on energy use, yield, transport and local prices were not available, and the thermal properties still require confirmation (Section 2.4). An indicative calculation is given instead, with its assumptions stated.

Table 18 and Figure 6 compare a 230 mm lining made from each retained composite with two commercial insulating firebricks and two published Nigerian clay bricks. Using the apparent conductivity at a nominal 1000 °C, the steady heat flux through a composite wall ranges from 5.20 kW/m^2 (A1) to 6.57 kW/m^2 (C3). This is similar to the flux through a dense Nigerian kaolinite brick (6.46 kW/m^2), but four to nine times that through JM26 (1.29 kW/m^2) and JM23 (0.74 kW/m^2). On these figures, the composites could not replace insulating firebrick as the main insulation layer of a continuously operated furnace.

Table 18. Indicative estimate for a 230 mm single-layer lining (hot face 1000 °C, cold face 100 °C)

Material	ρ (kg/m^3)	k (W/m·K)	m_A (kg/m^2)	q (kW/m^2)	Relative heat storage (%)
A1	1500	1.33	345	5.20	83
A2	1970	1.38	453	5.40	109
A3	1800	1.41	414	5.52	99
B1	1440	1.44	331	5.63	79
B2	1470	1.48	338	5.79	81
C2	1550	1.59	356	6.22	86
C3	2000	1.68	460	6.57	110
JM23 insulating firebrick [44]	480	0.19	110	0.74	26
JM26 insulating firebrick [44]	800	0.33	184	1.29	44
Nigerian kaolinite brick, 0% sawdust [14]	1812	1.65	417	6.46	100
Nigerian kaolinite brick, 40% sawdust [14]	1294	1.48	298	5.79	71

k for the composites is the apparent value at a nominal 1000 °C (Section 2.4); JM grades at 1000 °C; the published values for the Nigerian bricks were measured at a lower, unstated temperature. Relative heat storage = mA divided by mA of the 0% sawdust brick, assuming a similar mean specific heat for all materials. B3 and C1 omitted because their density is doubtful.

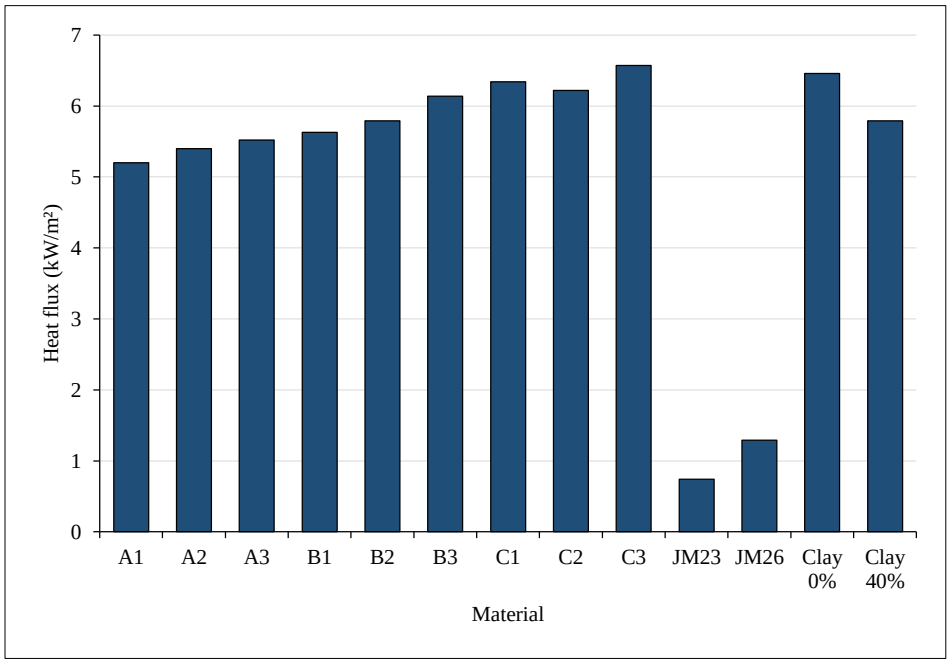


Fig. 6 Indicative steady heat flux through a 230 mm lining (hot face 1000 °C, cold face 100 °C), based on apparent conductivities, for the composites and reference materials

For intermittent kilns, heat stored in the lining is lost at every cycle, so lining mass also matters. On the assumption of a similar mean specific heat, the lighter composites (B1, B2 and A1) would store about 17 to 21% less heat per square metre than the dense Nigerian brick, whereas A2 and C3 would store about 10% more. Whether a lighter backup layer would shorten heating times or reduce fuel use in practice cannot be decided from these data; that would require confirmed thermal properties and measurements on an operating kiln.

On the production side, all formulations share the same firing schedule, so the firing energy per kilogram should be similar, and the energy per unit volume of lining should scale with bulk density; among the retained runs, B1 would need about 28% less than C3.

Absolute firing energy and emissions were not estimated in this revision, because the earlier estimate relied on the unconfirmed heat-capacity data. Once kiln fuel use has been measured, it can be converted to CO_2 with the default emission factor for natural gas [51]. The environmental case for the material rests on the use of local pumice and kaolin and on reduced dependence on imported shapes, not on low firing energy, since firing at 1200 °C is energy intensive. A cradle-to-gate LCA following ISO 14040 [52] is needed before an environmental advantage can be claimed.

3.9. Benchmarking against ASTM C155 and Published Materials

ASTM C155 classifies insulating firebrick by maximum bulk density together with a reheat change of no more than 2% after 24 h at the group temperature [39, 50]. None of the retained composites meets the density limits of Groups 16 to 30, which range from 0.54 to 1.09 g/cm^3. B1 (1.44 g/cm^3) and B2 (1.47 g/cm^3) fall below the 1.52 g/cm^3 limit of Groups 32 and 33, but those groups require dimensional stability at 1730 to 1790 °C, far above the 1200 °C reached in the cone test.

The composites, therefore, cannot be classed as insulating firebrick under ASTM C155. They are closer to lightweight fireclay-type refractories; whether they are suitable as backup or intermediate lining layers remains to be shown by load, reheat-change and service tests.

Table 19. Comparison with ASTM C155 limits, commercial insulating firebrick and published insulating materials

Material	ρ (g/cm^3)	P (%)	Strength (MPa)	k (W/m·K)	Basis
A1, present study	1.50	43.3	0.25 (flexural, as-fired)	1.33	Nominal 1000 °C, apparent
A2, present study	1.97	24.2	0.95 (flexural, as-fired)	1.38	Nominal 1000 °C, apparent
B2, present study	1.47	46.9	0.42 (flexural, as-fired)	1.48	Nominal 1000 °C, apparent
ASTM C155 Group 23 limit [39]	≤ 0.77	n.s.	n.s.	n.s.	Reheat ≤ 2% at 1230 °C
ASTM C155 Groups 32 and 33 limit [39]	≤ 1.52	n.s.	n.s.	n.s.	Reheat ≤ 2% at 1730 to 1790 °C
JM23 insulating firebrick [44]	0.48	n.r.	1.0 (MOR)	0.19	1000 °C
JM26 insulating firebrick [44]	0.80	n.r.	1.5 (MOR)	0.33	1000 °C
Clay brick with 40 wt% pumice [22]	n.r.	n.r.	n.r.	< 0.65	Ambient
Clay with pumice and vermiculite [23]	1.31	n.r.	n.r.	0.439	Ambient
Nigerian kaolinite brick, 40% sawdust [14]	1.29	n.r.	n.r.	1.48	Steady state
Mycelium bio-composites [53, 54]	n.r.	n.r.	n.r.	0.031 to 0.05	Ambient

n.s. = not specified by the standard; n.r. = not reported in the source; MOR = modulus of rupture.

The comparison with published work shows where the composites compare favourably and where they do not. Their apparent conductivity at a nominal 1000 °C (1.33 to 1.68 W/m·K) is of the same order as that of Nigerian kaolinite bricks with 0 to 40% sawdust (1.48 to 1.65 W/m·K) [14], and formulation A(1.50 g/cm^3) lies near the lower end of that range at a similar density without an organic pore former or burn-out stage, although the measurement temperatures differ and the comparison is indicative. Their as-fired flexural strength, at most 0.95 MPa (A2), is slightly below the modulus of rupture of JM23 (1.0 MPa) [44]. All nine formulations remained undeformed in the cone test up to 1200 °C, including those with 75 wt% pumice. The pumice-clay bricks of Gencel [22] and Koçyiğit [23] reached lower conductivities (below 0.65 W/m·K), but those values were measured at room temperature on bodies fired at 950 to 1000 °C for building use and cannot be compared directly with the present results. Bio-based insulators such as mycelium composites reach 0.031 to 0.05 W/m·K [53, 54], but they are combustible and serve a much lower temperature range; they illustrate how low the conductivity of low-temperature insulation can be, rather than offering an alternative refractory lining.

A likely reason why the composites fall short of insulating firebrick is that the vesicles that make pumice a good insulating aggregate may be largely opened by milling to 75 to 300 µm and closed by viscous flow of the pumice glass at 1200 °C. This explanation has not been tested by microscopy and is offered as a hypothesis. Commercial insulating firebricks obtain a fine, uniform pore structure from graded combustible fillers in a high-purity clay [44]. Two routes may narrow the gap and can be tested directly: using coarser pumice grains (1 to 3 mm) that retain their internal porosity, and firing at a lower temperature or adding alumina to limit glass formation.

3.10. Limitations and Future Work

Several limitations restrict how far these results can be applied. The L9 design was not replicated, so no estimate of pure error is available, and the residual includes any interaction between the factors. The water content, mixing time and pressing pressure of the green bodies were not recorded. For the thermal-shock tests, the temperature interval, quench medium, cycle count and reference strength were not documented, so the treated strengths are reported for completeness only, and the cyclic strength-loss data have been withdrawn.

The porosity and bulk density of B3 and C1 failed the apparent specific gravity check and could not be remeasured within the revision period, so those runs were excluded from the porosity- and density-based analyses, which then retain only two residual degrees of freedom. The heat capacities are mean values from drop calorimetry without a calorimeter correction and are treated as comparative. The conductivity apparatus details, calibration and heat-loss corrections are not documented, so the conductivities are apparent values at nominal temperatures.

No SEM, EDS, XRF or XRD data were obtained for the tested batches, the heating rate and reference-cone behaviour of the cone test were not recorded, and no RUL, creep or reheat-change tests were performed. Future work should prepare at least three specimens of each formulation, record all processing parameters, remeasure B3 and C1, carry out a documented water-quench thermal-shock test, confirm conductivity by laser flash and heat capacity by differential scanning calorimetry, add phase and microstructural analysis, perform RUL, creep and ASTM C210 reheat-change tests, measure conductivity as a function of moisture content, and test independent confirmation specimens at 25 wt% pumice with 75 and 150 µm particles.

4. Conclusion

Pumice-kaolin composites with 25 to 75 wt% pumice of 75 to 300 µm particle size were made from Nigerian raw materials, fired at 1200 °C and evaluated with a two-factor Taguchi L9 design. The main conclusion are as follows.

Bulk density (1.44 to 2.00 g/cm^3) increased with pumice content. Porosity varied non-monotonically between 24.2 and 46.9% among the seven formulations that passed an apparent specific gravity check; B3 and C1 failed this check and were excluded from the porosity- and density-based analyses.

Particle size had the largest effect on apparent thermal conductivity: moving from 75 to 300 µm raised it at a nominal 1000 °C from 1.37 to 1.63 W/m·K (85.8% contribution, p = 0.0008). As-fired flexural strength was lowest at 300 µm (mean 0.33 MPa against 0.69 MPa at 75 µm), but this effect was not statistically significant.

Grey relational analysis of the seven retained runs gave the highest grade to A1 (25 wt% pumice, 75 µm; 0.734), and A1 ranked first in ten of thirteen sensitivity scenarios. Factor-level analysis placed the preferred region at 25 wt% pumice with 75 to 150 µm particles.

Because the predicted and measured grades come from the same data, this is an internal fit check, and an independent replicated confirmation run is required. A2 (50 wt% pumice, 75 µm) is the alternative when strength is weighted more heavily.

No test cone deformed up to a kiln temperature of 1200 °C. The composites do not meet the ASTM C155 density limits for insulating firebrick, and their apparent conductivity is four to nine times that of commercial insulating firebrick grades, although it is of the same order as that of Nigerian insulating clay bricks. Their possible use as lightweight backup lining is therefore a preliminary indication only.

Replicated strength and thermal-shock tests, confirmed conductivity and heat-capacity measurements, phase and microstructural analysis, refractoriness under load, creep and reheat-change tests, moisture-dependent thermal measurements and a full life-cycle assessment are needed before any industrial use is considered.

Conflicts of Interest

The authors declare that there is no conflict of interest regarding the publication of this paper.

Funding Statement

This research received no external funding.

Acknowledgments

The authors thank the Nigerian Institute of Mining and Geosciences, Jos, and the Department of Physics, Ahmadu Bello University, Zaria, Nigeria, for access to their research facilities, and the technical staff of both institutions for their assistance with the experimental work.

References

[1] Kiyoshi Sugita, "*Historical Overview of Refractory Technology in the Steel Industry*," Nippon Steel Technical Report, no. 98, pp. 1-10, 2008. [Google Scholar] [Publisher Link]

[2] B.M. Thethwayo, and J.D. Steenkamp, "A Review of Carbon-Based Refractory Materials and their Applications," *Journal of the Southern African Institute of Mining and Metallurgy*, vol. 120, no. 11, pp. 641-650, 2020. [CrossRef] [Google Scholar] [Publisher Link]

[3] Reynaert Camille, Sniezek Edyta, and Szczerba Jacek, "Corrosion Tests for Refractory Materials Intended for the Steel Industry," *Ceramics-Silikaty*, vol. 64, no. 3, pp. 278-288, 2020. [CrossRef] [Google Scholar] [Publisher Link]

[4] S. Kamara, "A Summarized Review of Refractory Materials and their Chemical Components," *American Journal of Chemistry and Pharmacy*, vol. 4, no. 1, pp. 37-47, 2025. [CrossRef] [Google Scholar] [Publisher Link]

[5] Subir Biswas, *Refractory Materials: Processing, Properties and Applications*, 1st ed., Allied Publishers, 2022. [Google Scholar] [Publisher Link]

[6] Arup Ghosh, Somnath Sinhamahapatra, and Himansu Sekhar Tripathi, *Refractories as Advanced Structural Materials for High Temperature Processing Industries*, Future Landscape of Structural Materials in India, pp. 279-292, 2022. [CrossRef] [Google Scholar] [Publisher Link]

[7] Mohamed Lokman Jalaluddin et al., "A Review of Pore-Forming Agents on the Structures, Porosities, and Mechanical Properties of Porous Ceramics," *AIMS Materials Science*, vol. 11, no. 4, pp. 634-665, 2024. [CrossRef] [Google Scholar] [Publisher Link]

[8] Chinwuba Victor Ossia, and Mathew Uzoma Shedrack, "Optimization of Blast Furnace Throughput Based on Hearth Refractory Lining," *Journal of Casting and Materials Engineering*, vol. 5, no. 1, pp. 5-13, 2021. [CrossRef] [Google Scholar] [Publisher Link]

[9] Oluwagbenga Peter Odewole, and Emmanuel Majiyebo Alemaka, "Development of Aluminosilicate Refractory Crucibles from Awo Quartz and Ikere Ekiti Clays," *Journal of Science, Technology and Education*, vol. 7, no. 2, pp. 1-10, 2019. [Publisher Link]

[10] Peter Oluwagbenga Odewole, Isah Bolaji Kashim, and Tolulope Lawrence Akinbogun, "Production of Refractory Porcelain Crucibles from Local Ceramic Raw Materials using Slip Casting," *International Journal of Engineering and Manufacturing*, vol. 9, no. 5, pp. 56-69, 2019. [CrossRef] [Google Scholar] [Publisher Link]

[11] P.O. Atanda, O.O. Oluwole, and T.A. Oladeji, "Electrical Porcelain Production from Selected Kaolin Deposits in South Western Nigeria using Slip Casting," *International Journal of Materials and Chemistry*, vol. 2, no. 3, pp. 86-89, 2012. [CrossRef] [Google Scholar] [Publisher Link]

[12] Oladimeji Rabiu Ishola, "Effect of Additives on Refractory Properties of Some Selected Clay Deposits in Niger State, Nigeria," *Masters Theses*, Federal University of Technology, pp. 1-100, 2022. [Google Scholar] [Publisher Link]

[13] Eugenia Obidiegwu, Henry E. Mgbemere, and Arhuere O. Akporehe, "The Study of Insulating Properties of Refractory Bricks Produced using Melon Seed Husks as Pore Former," *Kufa Journal of Engineering*, vol. 15, no. 2, pp. 61-73, 2024. [CrossRef] [Google Scholar] [Publisher Link]

[14] Chigbo A. Mgbemene, Esther T. Akinlabi, and Omolayo M. Ikumapayi, "Dataset Showing Thermal Conductivity of South-Eastern Nigerian Kaolinite Clay Admixtures with Sawdust and Iron Filings for Fired-Bricks Production," *Data in Brief*, vol. 27, pp. 1-10, 2019. [CrossRef] [Google Scholar] [Publisher Link]

[15] Alaa M. Rashad, "A Short Manual on Natural Pumice as a Lightweight Aggregate," *Journal of Building Engineering*, vol. 25, 2019. [CrossRef] [Google Scholar] [Publisher Link]

[16] *Mineral Commodity Summaries 2020*, U.S. Geological Survey, 2020. [CrossRef] [Google Scholar] [Publisher Link]

[17] Fatemeh Mobasheri et al., "Durability and Mechanical Properties of Pumice-based Geopolymers: A Sustainable Material for Future," *Iranian Journal of Science and Technology, Transactions of Civil Engineering*, vol. 46, no. 1, pp. 223-235, 2022. [CrossRef] [Google Scholar] [Publisher Link]

[18] Karan Moolchandani, "Advancements in Pumice-Based Concrete: A Comprehensive Review," *Next Materials*, vol. 8, pp. 1-13, 2025. [CrossRef] [Google Scholar] [Publisher Link]

[19] Maria Nomikou et al., "Master Floor: The New Application of Pumice Stone as Lightweight Floor Filling Material," *Materials Proceedings*, vol. 5, no. 1, pp. 1-4, 2021. [CrossRef] [Google Scholar] [Publisher Link]

[20] Agnieszka Przybek et al., "Thermal Properties of Geopolymer Concretes with Lightweight Aggregates," *Materials*, vol. 18, no. 13, pp. 1-30, 2025. [CrossRef] [Google Scholar] [Publisher Link]

[21] Abdullah M. Zeyad, and Ali Almalki, "Role of Particle Size of Natural Pozzolanic Materials of Volcanic Pumice: Flow Properties, Strength, and Permeability," *Arabian Journal of Geosciences*, vol. 14, no. 2, 2021. [CrossRef] [Google Scholar] [Publisher Link]

[22] Osman Gencel, "Characteristics of Fired Clay Bricks with Pumice Additive," *Energy and Buildings*, vol. 102, pp. 217-224, 2015. [CrossRef] [Google Scholar] [Publisher Link]

[23] Fatih Koçyiğit et al., "Thermo-Physical and Mechanical Properties of Clay Bricks Produced for Energy Saving," *International Journal of Thermophysics*, vol. 43, no. 2, 2022. [CrossRef] [Google Scholar] [Publisher Link]

[24] W.E. Lee et al., "Mullite Formation in Clays and Clay-Derived Vitreous Ceramics," *Journal of the European Ceramic Society*, vol. 28, no. 2, pp. 465-471, 2008. [CrossRef] [Google Scholar] [Publisher Link]

[25] H. Schneider, J. Schreuer, and B. Hildmann, "Structure and Properties of Mullite: A Review," *Journal of the European Ceramic Society*, vol. 28, no. 2, pp. 329-344, 2008. [CrossRef] [Google Scholar] [Publisher Link]

[26] C.Y. Chen, G.S. Lan, and W.H. Tuan, "Microstructural Evolution of Mullite during the Sintering of Kaolin Powder Compacts," *Ceramics International*, vol. 26, no. 7, pp. 715-720, 2000. [CrossRef] [Google Scholar] [Publisher Link]

[27] Alima Mebrek et al., "Development of Composite Ceramics with Kaolin and Spent Refractory Bricks," *JOM*, vol. 75, no. 12, pp. 5808-5818, 2023. [CrossRef] [Google Scholar] [Publisher Link]

[28] Amadou Pountouenchi et al., "Characterization of Refractory Bricks from Selected Cameroonian Kaolins," *Clay Minerals*, vol. 58, no. 4, pp. 353-363, 2023. [CrossRef] [Google Scholar] [Publisher Link]

[29] Jagadiswar Reddy Tippi Reddy, Jens Schuster, and Yousuf Pasha Shaik, "Development of Kaolin and Glass Fiber Reinforced Composites for Thermal Insulating Panels," *Open Journal of Composite Materials*, vol. 14, no. 1, pp. 44-59, 2024. [CrossRef] [Google Scholar] [Publisher Link]

[30] David S. Smith et al., "Thermal Conductivity of Porous Materials," *Journal of Materials Research*, vol. 28, no. 17, pp. 2260-2272, 2013. [CrossRef] [Google Scholar] [Publisher Link]

[31] Ya-Wen Lin et al., "Characteristics of Functional Water Retaining Porous Ceramics Prepared from Waste Diatomite and Waste Ceramics Tiles," *Ceramics International*, vol. 50, no. 5, pp. 8065-8072, 2024. [CrossRef] [Google Scholar] [Publisher Link]

[32] Anna Szymczak-Graczyk et al., "Application of Experimental Studies of Humidity and Temperature in the Time Domain to Determine the Physical Characteristics of a Perlite Concrete Partition," *Materials*, vol. 17, no. 19, pp. 1-21, 2024. [CrossRef] [Google Scholar] [Publisher Link]

[33] Bianlei Hao et al., "Heat Transfer Mechanism and Performance Optimization Scheme of Refractory Oxide Solid Heat Storage Materials," *Ceramics International*, vol. 50, no. 12, pp. 21686-21694, 2024. [CrossRef] [Google Scholar] [Publisher Link]

[34] Phillip J. Ross, *Taguchi Techniques for Quality Engineering Loss Function, Orthogonal Experiments, Parameter and Tolerance Design*, 2nd ed., McGraw-Hill, New York, 1996. [Google Scholar] [Publisher Link]

[35] Douglas C. Montgomery, *Design and Analysis of Experiments*, 9th ed., John Wiley and Sons, pp. 1-630, 2017. [Google Scholar] [Publisher Link]

[36] Deng Julong, "Introduction to Grey System Theory," *The Journal of Grey System*, vol. 1, no. 1, pp. 1-24, 1989. [Google Scholar] [Publisher Link]

[37] S. A. J. Al-Sultani, I. A. Disher Al-Hydary, and M. A. Ahmed Al-dujaili, "Taguchi-Grey Relational Analysis for Optimizing the Compressive Strength and Porosity of Metakaolin-Based Geopolymer," *International Journal of Engineering, Transactions B: Applications*, vol. 34, no. 11, pp. 2525-2533, 2021. [CrossRef] [Google Scholar] [Publisher Link]

[38] Minseok Nam et al., "Multi-Response Optimisation of Quaternary Blended Mortar using Taguchi-Grey Relational Analysis," *International Journal of Concrete Structures and Materials*, vol. 19, 2025. [CrossRef] [Google Scholar] [Publisher Link]

[39] ASTM C155-97, *Standard Classification of Insulating Firebrick*, Advancing Standards Transforming Markets International, pp. 1-2, 2022. [CrossRef] [Publisher Link]

[40] ASTM C20-00, *Standard Test Methods for Apparent Porosity, Water Absorption, Apparent Specific Gravity, and Bulk Density of Burned Refractory Brick and Shapes by Boiling Water*, Advancing Standards Transforming Markets International, pp. 1-3, 2015. [CrossRef] [Google Scholar] [Publisher Link]

[41] ASTM C1161-18, *Standard Test Method for Flexural Strength of Advanced Ceramics at Ambient Temperature*, Advancing Standards Transforming Markets International, pp. 1-19, 2018. [CrossRef] [Publisher Link]

[42] ASTM C24-01, *Standard Test Method for Pyrometric Cone Equivalent (PCE) of Fireclay and High Alumina Refractory Materials*, Advancing Standards Transforming Markets International, 2001. [CrossRef] [Publisher Link]

[43] Yanfeng Jiang et al., "High-Temperature Mechanical Properties and Thermal Shock Resistance of an Alumina-Fiber-Reinforced Alumina Ceramic Matrix Composite," *Ceramics International*, vol. 51, no. 4, pp. 5459-5469, 2025. [CrossRef] [Google Scholar] [Publisher Link]

[44] JM® Insulating Firebrick Series: Product Data Sheet, Morgan Advanced Materials, 2025. [Online]. Available: https://www.morganthermalceramics.com/media/5beap13n/jm-ifb-series_eng.pdf

[45] Barbara Ksit et al., "Numerical and Surrogate Modeling of Drying Processes in Building Envelopes under Variable Climatic Conditions," *Energy*, vol. 339, 2025. [CrossRef] [Google Scholar] [Publisher Link]

[46] Mateusz Smoczyk, Barbara Ksit, and Anna Szymczak-Graczyk, "Numerical Analysis of the Ground Temperature Function Depending on Edge Thermal Insulation Parameters for Shallow Slab Foundations," *Energy*, vol. 314, 2025. [CrossRef] [Google Scholar] [Publisher Link]

[47] ISO 1893:2005, *Refractory Products: Determination of Refractoriness-Under-Load, Differential Method with Rising Temperature*, International Organization for Standardization, 2005. [Google Scholar] [Publisher Link]

[48] ASTM C832, *Standard Test Method of Measuring Thermal Expansion and Creep of Refractories Under Load*, Advancing Standards Transforming Markets International, pp. 1-7, 2006. [CrossRef] [Publisher Link]

[49] Michel Henze et al., "Determination of Temperature Dependent Static Young's Modulus of Refractory Ceramics using RUL Tests," *International Journal of Ceramic Engineering and Science*, vol. 4, no. 2, pp. 77-83, 2022. [CrossRef] [Google Scholar] [Publisher Link]

[50] ASTM C210-95, *Standard Test Method for Reheat Change of Insulating Firebrick*, Advancing Standards Transforming Markets International, 2024. [CrossRef] [Publisher Link]

[51] IPCC, 2006 IPCC Guidelines for National Greenhouse Gas Inventories, Intergovernmental Panel on Climate Change, 2006. [Online]. Available: https://www.ipcc-tfi.iges.or.jp/meeting/pdfiles/Washington_Report.pdf

[52] ISO 14040:2006, *Environmental Management: Life Cycle Assessment, Principles and Framework*, International Organization for Standardization, 2006. [Google Scholar] [Publisher Link]

[53] Ilze Luksta, Ilze Vamža, and Dagnija Blumberga, "Development of a Mycelium-Based Thermal Insulation Material," *Environmental and Climate Technologies*, vol. 29, no. 1, pp. 201-211, 2025. [CrossRef] [Google Scholar] [Publisher Link]

[54] Joni Wildman et al., "Comparing Substrates for Mycelium-Based Composite Insulation Materials with Thermal and Environmental Assessment," *Scientific Reports*, vol. 16, pp. 1-19, 2026. [CrossRef] [Google Scholar] [Publisher Link]